Detection and characteristics estimation of defects in concrete structures using laser ablation-induced vibration

Naotoshi Yasuda[a,*], Norikazu Misaki[b], Yoshinori Shimada[c], Daiki Yamaoka[a]

[a] *Department of Civil and Earth Resources Engineering, Kyoto University, Katsura, Nishikyo-ku, Kyoto 615-8530, Japan*
[b] *West Japan Railway Company, Shibata, Kita-ku, Osaka 530-8341, Japan*
[c] *Institute for Laser Technology, Yamadaoka, Suita-shi, Osaka 565-0871, Japan*

Abstract

This paper proposes a method for detection and estimation of the characteristics of defects in concrete structures using laser ablation-induced vibration for non-contact structural inspection to prevent partial spalling. Two types of lasers are used: the first is an impact laser that is used to induce vibrations in the measurement target and the second is a detection laser that is used to measure these induced vibrations. Laboratory tests are performed using concrete specimens with and without an internal defect. The results show that the presence of a defect can be estimated from the occurrence of damped oscillations in the measurement data. The presence or absence of these damped oscillations can be determined using the least-squares complex frequency-domain (LSCF) method, which is a fast-stabilizing parameter estimation method for modal identification problems. Additionally, when a defect is present, the defect vibration characteristics, such as natural fre-

*Corresponding author. Tel.:+81 75 383 7558; Fax: +81 75 383 3114
Email address: yasuda.naotoshi.3x@kyoto-u.ac.jp (Naotoshi Yasuda)

quencies and damping ratios, can be estimated. In particular, the natural frequencies can be estimated accurately.
Keywords: inspection method, laser ablation, concrete, vibration, modal identification

1. Introduction

Most modern infrastructure, including bridges, viaducts, buildings, dams, and tunnels, is mainly constructed from concrete. To maintain the functions of these structures and prevent accidents, periodic inspections are necessary. For example, in Japan in 1999, a concrete lining block in the Fukuoka tunnel spalled and the block hit a Shinkansen train (Asakura and Kojima, 2003). This accident served as a reminder of the importance of maintenance and careful periodic inspections thus became mandatory.

One of the most commonly used methods for the inspection of concrete structures is the hammering test, in which an inspector strikes a target using a steel hammer and evaluates the spalling risk using human sensory abilities such as auditory sensation and tactile sensation. This approach is widely used as an inspection method because it is easy to perform and it can be used to chip areas of concrete that are already at risk of spalling on the spot. However, there are some problems with this test such as the lack of skilled technicians, the risk of falling from high places, and the lack of unified evaluation criteria. Recently, to address these problems, researchers have proposed approaches that include an infrared method (Sakagami and Kubo, 2002; Clark et al., 2003; Maierhofer et al., 2006; Meola, 2007; Afshani et al., 2019), a non-contact acoustic exploration method (Mori et al., 2002; Zhu and

Popovics, 2007; Akamatsu et al., 2013; Sugimoto et al., 2015), and a remote laser sensing method (Kotyaev et al., 2006; Kurahashi et al., 2018) that would enable mechanization, non-contact testing, and objective evaluation of the results.

In the mechanical methods described above, specific index values are defined for evaluation purposes, including the relative ratio of the peak value to the average value in the measured frequency spectrum (Kurahashi et al., 2018), vibrational energy ratio, and spectrum entropy (Sugimoto et al., 2015). By creating contour maps from these values, the presence or absence of defects and their positions and sizes can be estimated. However, the signal, which is the measurement data caused by the presence of defects, is often not so high in the non-contact testing case. When the signal is low, these index values often do not work well because it can not be distinguished the signal and the other responses such as electrical noise and vibration of the measurement device. Additionally, the relationship between these index values and the degree of risk of spalling, which is the original purpose of the inspection, remains unclear because these values lack physical meaning.

In the remote laser sensing method, a pulsed laser with a very short radiation time is used as the excitation source. Therefore, the measurement results may be regarded as an impulse response (Kajiwara and Hosoya, 2011; Hosoya et al., 2012), that represents the vibration characteristics of the defect. In addition, because the hammering sound, especially the presence of low and dull sound, is used for the inspection, there is a strong relationship between the defect's vibration characteristics and the degree of risk of spalling.

This paper presents a method for detection and estimation of the characteristics of defects in concrete structures using the remote laser sensing method. Laboratory tests are performed using concrete specimens with and without an internal defect. The laser-induced vibration characteristics of the defective parts are investigated and are extracted for use in inspections.

2. Outline of remote laser sensing method

Fig. 1 shows a schematic diagram of the proposed remote laser sensing method. Two types of lasers are used: the first is an "impact laser" used to induce vibrations in the measurement target and the second is a "detection laser" used to measure these induced vibrations. The impact laser is a high-power pulsed Nd:YAG laser (SLT-ND-EOQ-AMR, Sparkling Photon) with a wavelength of 1064 nm and pulse width of approximately 10 ns. This laser is used to excite laser ablation, which is the process of material removal from a solid surface by high-power pulsed laser irradiation. The detection laser is a laser Doppler vibrometer (RSV-150, Polytec). The sensor head is placed on the supplied tripod.

3. Experimental study

3.1. Outline of experiment

Fig. 2 shows the dimensions of a concrete specimen containing an internal defect that is used in the laboratory tests. The specimen is 450 mm wide, 450 mm long, 150 mm thick and weighs approximately 70 kg. These dimensions were adopted to ensure specimen portability. The internal defect is modeled from Styrofoam, is 300 mm long, 300 mm wide, 5 mm thick and is

located at a depth of 20 mm from the surface. Another concrete specimen with no such internal defect is also prepared.

Table 1 summarizes the concrete mix proportions. The compressive strength of the concrete specimen is approximately 27 $\mathrm{N/mm^2}$ at 28 days old. The concrete specimen used in this study is quite artificial. However, the resulting considerations are not affected by the defect structure as long as the abnormal sound can be heard after the hammer strikes.

Fig. 3 shows the impact point and the measurement points on the concrete specimen. In this study, a impact point is fixed to estimate vibration mode shapes and investigate the validity of the estimated results later. The position is chosen to avoid nodes of main vibration modes. The impact laser irradiation is used as a trigger to synchronize vibration measurements at each point. There are a total of 121 measurement points spaced at constant intervals. Locations A to D are specified as measurement points for more detailed discussion later. Concrete specimen was placed on natural rubber sheet, which is 450 mm wide, 450 mm long and 10 mm thick, to prevent rattling.

Data acquisition is performed at a sampling frequency of 100 kHz with no filter. The distance between the measurement device and the concrete specimens is 5.0 m, which is consistent with measurements being performed in a Shinkansen train tunnel. The impact laser energy in front of the specimen is approximately 3.6 J.

3.2. Results and discussion

3.2.1. Characteristics of laser-induced vibration caused by defect

Fig. 4 compares the laser-induced vibrations in the concrete specimen with the internal defect and that without the defect at measurement point

A. Fig. 4(a) shows the velocity waveform when averaged over five measurements, which covers 0.10 s (10000 measurement data points). The impact laser is radiated at 0.0020 s. Fig. 4(b) shows the Fourier spectrum of the velocity waveform. When a defect is present, damped oscillation is observed immediately after laser ablation. This oscillation includes some oscillation modes because characteristic peaks can be observed in the Fourier amplitude spectrum. These peaks are mainly due to flexural vibration of the defect. In contrast, when no defect is present, it is difficult to recognize a damped oscillation from the velocity waveform. In the Fourier phase spectrum, a characteristic waveform can be seen, regardless of the presence or absence of the internal defect. This is mainly caused by a dead time including the measurement data (Hosoya et al., 2012), which is the 0.0020 s before laser radiation starts. The dead time should be removed to avoid obtaining incorrect phase characteristics. In addition, the pulse-like response in the velocity waveform that always occurs immediately after laser ablation. This is not the actual vibration of the concrete specimen; instead, it is caused by an instantaneous reduction in the reflected detection laser light, which is caused by materials removed from a concrete surface by laser ablation such as dust, plasma emission, and a compressional wave in the atmosphere. Therefore, measurement data acquired slightly after laser ablation should be used for evaluation. It should also be noted that the spectrum peak around 1800 Hz is not a natural defect vibration but is a natural vibration of the laser Doppler vibrometer with the tripod. The maximum damped wave amplitude is approximately 70 nm when converted into a displacement and is thus quite small. Therefore, the measurement results are susceptible to disturbance from the surrounding

environment such as the wind and the sound from the machines, which are inevitable at the site.

Fig. 5 shows the laser-induced vibrations at measurement point A when an internal defect is present. The data begins 0.0010 s after laser irradiation starts. Fig. 5(a) shows the velocity waveforms for five measurements and covers a period of approximately 0.082 s (8192 measurement data points). Fig. 5(b) shows the Fourier spectra of these waveforms. The acquired data indicates the high repeatability of the laser ablation procedure. The phase change within the vicinity of the natural frequency can be evaluated well by removing the data acquired immediately after irradiation.

3.2.2. Method for estimation of the presence or absence of damped oscillations

As mentioned in the previous section, damped oscillations are observed when a defect is present. Therefore, detection of these damped oscillations can be used as an indicator of the defect's presence. A method for estimation of the presence or absence of the damped oscillations is presented below.

Let $f_{k(t_j)}$ be a waveform measured at measurement point k with a fixed impact point. The estimation formula $f'_{k(t_j)}$ represents the sum of the damped oscillations and is given as follows:

$$f'_{k(t_j)} = 2\mathrm{Re}\left[\sum_{n=1}^{N} A_{kn} e^{S_n t_j}\right] = \sum_{n=1}^{N} \left(A_{kn} e^{S_n t_j} + A^*_{kn} e^{S^*_n t_j}\right), \text{where} \quad (1)$$

$$S_n = -\xi_n \omega_n + i\sqrt{1-\xi_n^2}\,\omega_n = 2\pi f_n(-\xi_n + i\sqrt{1-\xi_n^2}); \quad (2)$$

N is the number of assumed oscillation modes; A_{kn} is the complex amplitude of the nth oscillation mode at measurement point k; t_j is the time at which the

jth datum is acquired; and ω_n, f_n, and ξ_n are the natural angular frequency, the natural frequency, and the damping ratio of the nth vibration mode, respectively. The superscript * denotes the complex conjugate.

For a specified number of assumed modes N, the evaluation function g can be written as:

$$g = \sum_{k=1}^{K} \sum_{j=1}^{J} |f_{k(t_j)} - f'_{k(t_j)}|^2, \tag{3}$$

where K is the total number of measurement points and J is the total number of data acquired at each measurement point. The evaluation function g is zero when there is no noise present and increases according to the noise level. Values of A_{kn}, ξ_n, and ω_n that minimize g can be determined uniquely (Spitznogle and Quazi, 1970). These estimated parameters are dependent on the value of N. When the estimated parameters do not change significantly, regardless of the N value, it can be determined that the damped oscillations actually exist.

In theory, there is no problem with the above method. However, it is difficult to apply in practice because the solution tends to become unstable by the presence of noise. Therefore, in this paper, the least-squares complex frequency-domain (LSCF) method (Van Der Auweraer et al., 2001; Verboven et al., 2004), which is a type of parameter estimation method for modal identification problems, is used for the estimation. This method is described briefly below.

The estimated transfer function $X'_{k(z)}$, which is derived from the Z-

transform of Eq. (1), can be written as follows:

$$X'_{k(z)} = \sum_{n=1}^{N} \left(\frac{A_{kn}}{1 - e^{S_n T_s} z^{-1}} + \frac{A^*_{kn}}{1 - e^{S^*_n T_s} z^{-1}} \right) \tag{4}$$

$$= \frac{\sum_{n=1}^{2N} B_{kn} z^{-n}}{\sum_{n=1}^{2N} C_n z^{-n}}, \tag{5}$$

where B_{kn} and C_n are real-valued coefficients and T_s is the sampling period. The transfer function poles can be derived from the following equations after the coefficient C_n is determined:

$$\sum_{n=1}^{2N} C_n z^{-n} = 0. \tag{6}$$

From Eqs. (2) and (4), it is found that the natural frequency and the damping ratio of the nth vibration mode can be derived from the identified poles.

The estimated frequency response function $H'_{k(\omega_f)}$, which is obtained by substituting $e^{i\omega_f T_s}$ into z in Eq. (5), can be defined as follows:

$$H'_{k(\omega_f)} = \frac{\sum_{n=1}^{2N} B_{kn} e^{-i\omega_f T_s n}}{\sum_{n=1}^{2N} C_n e^{-i\omega_f T_s n}} = \frac{N_k(\omega_f)}{D(\omega_f)}, \tag{7}$$

where ω_f is the discrete angular frequency. The estimated solutions for B_{kn} and C_n are obtained by minimizing the evaluation function h:

$$h = \sum_{k=1}^{K} \sum_{f=1}^{F} \left| H_{k(\omega_f)} - H'_{k(\omega_f)} \right|^2 = \sum_{k=1}^{K} \sum_{f=1}^{F} \left| H_{k(\omega_f)} - \frac{N_k(\omega_f)}{D(\omega_f)} \right|^2, \tag{8}$$

where $H_{k(\omega_f)}$ is the Fourier spectrum of $f_k(t_j)$, and F is the number of data from the spectrum used in the estimation process.

However, Eq. (8) has a strong nonlinearity and is thus difficult to solve. Therefore, it is assumed that $h \approx 0$ and the following equation can be solved:

$$\sum_{k=1}^{K} \sum_{f=1}^{F} \left| D(\omega_f) H_{k(\omega_f)} - N_k(\omega_f) \right|^2. \tag{9}$$

As a result, the estimated solutions can be derived by solving a linear problem. In addition, a fast Fourier transform algorithm can be used in the calculation process and C_n can be derived without deriving B_{kn}. Therefore, the solution is stable and the calculation speed is high.

3.2.3. Evaluation of estimated solutions

The estimated solutions can be verified using a stabilization diagram. Fig. 6 shows the stabilization diagrams obtained following application of the LSCF method. Fig. 6(a) is derived from the spectrum shown in Fig. 5(b). Fig. 6(b) shows the case where the specimen has no defect. The horizontal axis represents the frequency and the vertical axis represents the assumed order of the model. In these figures, the estimated natural frequencies are visualized for the different model orders. The frequencies used to perform the estimation range from approximately 300 Hz to 3400 Hz. The upper limit was determined with reference to the main frequency range of excited vibration in hammering test, which is less than 4kHz. The number of data points from the spectrum used for estimation F is 128. This figure is not derived from an average of five measurements but instead from five different measurements. The red line represents the amplitude spectrum, which is the average of five shots. The symbols $*$, $\triangle$, and $\circ$ indicate when the estimated solution is physically meaningful, i.e., when both the frequency and the damping ratio derived from a pole are positive. This distinction is based on the relationship between the estimated solutions and those obtained from the previous model order: $*$ corresponds to a new pole, $\triangle$ indicates that the pole frequency is close to its previous value (frequency within 2%) and $\circ$ indicates that both the frequency and the damping ratio are close to their previous

values (frequency within 2% and damping ratio within 5%). The stability of the estimated solutions can then be inferred from the arrangement of these symbols. When the symbols $*$, $\triangle$ or $\circ$ are arrayed vertically in a column, the estimated solutions are stable and reliable. It is expected that two types of damped oscillation mode will be included in the laser-induced vibrations in the concrete specimen with the internal defect. In particular, the estimated solutions around 1200 Hz are very stable and reliable because the symbol $\circ$ arrayed vertically in a column. In contrast, there are no symbols for the case with no defects. The peak around 1800 Hz, which is the natural frequency of the measurement device itself, is not regarded as a physically meaningful solution because it is continuous vibration rather than damped oscillation.

Fig. 7 shows the laser-induced vibration results obtained from the concrete specimen with the internal defect at measurement points B, C, and D. The data begins 0.0010 s after laser irradiation starts. Fig. 7(a) shows the velocity waveforms when averaged over five measurements and Fig. 7(b) shows the Fourier spectra of these waveforms. Points B and C are located over the defective area and point D is located slightly away from this area. Damped oscillation is observed at points B and C and several characteristic spectrum peaks can be seen. In contrast, at point D, it is difficult to recognize clear damped oscillations or mountain-shaped spectrum peaks and phase changes that represent damped oscillations.

Fig. 8 shows the stabilization diagrams for the laser-induced vibrations at measurement points B, C, and D. These figures were derived in the same way as those in Fig. 6. At both points B and C, numerous symbols are arrayed vertically at several frequencies. These estimated solutions are reliable.

However, the estimated solution around 2000 Hz at point C is less stable than that at point B because the excited vibration at point C is smaller than that at point B. At point D, there are only a few symbols around 2200 Hz. This makes it difficult to judge the validity of the estimated solution using the result alone. When the results from points B and C are considered, the estimated solution appears to be reliable. In this experiment, when the results at other points are considered, an estimation result could be judged as reliable when four or more symbols are arrayed vertically in a column.

Fig. 9 shows the distribution of the estimated natural frequencies and damping ratios of the defect. The number of assumed modes N used for the calculation ranges from 28 to 32 for each point. The natural frequencies can be estimated accurately. When compared with the frequencies, the estimation accuracy of damping ratios is low.

As described above, it is possible to determine the presence or absence of defects using the LSCF method. Additionally, when a defect is present, the defect vibration characteristics, such as natural frequencies and damping ratios, can be estimated. Note here that the amplitude of each mode can also be estimated. However, the amplitude value is not determined by the defect structure alone. It depend on excitation point, measurement point, performance of impact laser and surface condition of the concrete. Therefore, the amplitude appears to be less important for use in inspections.

Fig. 10 shows the Fourier amplitude spectra for the concrete specimen with the internal defect that were measured at all 121 points. The value given for each point is the average of five measurements. There are four main peaks at around 1200 Hz, 2100 Hz, 2200 Hz, and 3200 Hz. One spectrum that

was more unstable than the others was measured at one point below point B. This is because the materials removed from a solid surface by laser ablation obstruct the reflected detection laser light. Therefore, the impact laser and the detection laser must remain a certain distance apart.

Fig. 11 shows the stabilization diagrams derived from all 121 points. The red line represents the amplitude spectrum, which is an average of the 121 points. Five mode types appear and the estimated indicators for these modes are given in Table 2. These results are for an assumed mode number of $N = 32$. Fig. 12 shows the estimated mode shapes. Eq. (1) is used with the estimated indicators listed in Table 2 to perform mode shape estimation. The vertical axis represents the estimated maximum velocity amplitude, which is the value calculated when ignoring the effect of the attenuation term. With the exception of mode 2, the upper part of the defect vibrates and almost no vibration occurs on the defect-free part. Mode 2 is the vibration mode that has little relation to the defect. In actual concrete structures, such a mode cannot be measured because these structures are much larger in size than the concrete specimen and the amplitude of the laser induced vibration becomes too small to be measured.

Fig. 13 shows the modal assurance criterion (MAC) values calculated between each of the estimated modes. These MAC values are calculated using the following equations:

$$\mathrm{MAC}_{ij} = \frac{\sum_{k=1}^{121} A_{ki} A_{kj}}{\sum_{k=1}^{121} A_{ki} A_{ki} \sum_{k=1}^{121} A_{kj} A_{kj}}, \tag{10}$$

where A_{ki} and A_{kj} are the complex amplitude as shown in Eq. (1). The non-diagonal components of these MAC values are almost zero. This means that each estimated mode has orthogonality. Therefore, the validity of the

estimated results was confirmed.

In this study, the excitation point is fixed and only the measurement points are moved to estimate vibration mode shapes and investigate the validity of the estimated results. However, mode shape estimation takes considerable time and is less important for evaluating the degree of risk of spalling, which is the original purpose of the inspection. Therefore, there is little need to fix the excitation points or the measurement points in actual inspections.

There is a considerable difference in excited vibration magnitude between the data from the defective area and those from the nondefective area as shown in Fig. 12. To investigate the presence or absence of damped oscillations based on better quality data, both the excitation points and the measurement points should be located in the areas where defects are likely to exist, e.g., the area around a crack.

4. Conclusions

This paper has presented a method for detection and estimation of the characteristics of defects in concrete structures using laser ablation-induced vibration. Laboratory tests were performed using a concrete specimen with and without an internal defect. The laser-induced vibration characteristics of the defective parts were investigated and were extracted for use in inspections. The following conclusions can be drawn from this study:

(1) When a defect is present, damped oscillation caused by flexural vibration of the defective part is observed immediately after laser ablation.

Therefore, detection of these damped oscillations can be used as an indicator of the presence of a defect.

(2) Application of the LSCF method, which is a fast-stabilizing parameter estimation method for modal identification problems, to the measurement results allows stabilization diagrams to be obtained. Using these diagrams, it is possible to determine the presence or absence of a defect. Additionally, when a defect is present, the defect vibration characteristics, such as the natural frequencies and damping ratios, can be estimated.

(3) Natural frequencies can be estimated accurately. When compared with the frequencies, the estimation accuracy of damping ratios is low.

(4) The impact laser and the detection laser must remain a certain distance apart because materials removed from a solid surface by laser ablation obstruct the reflected detection laser light.

(5) Both the excitation point and the measurement point should be located in the areas where defects are likely to exist, such as the area around a crack, to investigate the presence or absence of damped oscillations based on better quality data.

The usefulness of this method was verified via laboratory testing using concrete specimens with and without an internal defect. Non-contact inspection of these concrete structures was realized using the proposed method. The relationships between the natural frequencies and damping ratios of a defect and the degree of risk of spalling will have to be considered in future work.

References

Afshani, A., Kawakami, K., Konishi, S., Akagi, H., 2019. Study of infrared thermal application for detecting defects within tunnel lining. Tunnelling and Underground Space Technology 86, 186 – 197.

Akamatsu, R., Sugimoto, T., Utagawa, N., Katakura, K., 2013. Proposal of non contact inspection method for concrete structures using high-power directional sound source and scanning laser doppler vibrometer. Japanese Journal of Applied Physics 52, 07HC12.

Asakura, T., Kojima, Y., 2003. Tunnel maintenance in japan. Tunnelling and Underground Space Technology 18, 161 – 169.

Clark, M., McCann, D., Forde, M., 2003. Application of infrared thermography to the non-destructive testing of concrete and masonry bridges. NDT & E International 36, 265 – 275.

Hosoya, N., Kajiwara, I., Hosokawa, T., 2012. Vibration testing based on impulse response excited by pulsed-laser ablation: Measurement of frequency response function with detection-free input. Journal of Sound and Vibration 331, 1355 – 1365.

Kajiwara, I., Hosoya, N., 2011. Vibration testing based on impulse response excited by laser ablation. Journal of Sound and Vibration 330, 5045 – 5057.

Kotyaev, O., Shimada, Y., Hashimoto, K., et al., 2006. Laser-based non-destructive detection of inner flaws in concrete with the use of lamb waves,

in: European Conference for Non Destructive Testing, September, pp. 25–29.

Kurahashi, S., Mikami, K., Kitamura, T., Hasegawa, N., Okada, H., Kondo, S., Nishikino, M., Kawachi, T., Shimada, Y., 2018. Demonstration of 25-hz-inspection-speed laser remote sensing for internal concrete defects. Journal of Applied Remote Sensing 12, 015009.

Maierhofer, C., Arndt, R., Röllig, M., Rieck, C., Walther, A., Scheel, H., Hillemeier, B., 2006. Application of impulse-thermography for non-destructive assessment of concrete structures. Cement and Concrete Composites 28, 393 – 401.

Meola, C., 2007. A new approach for estimation of defects detection with infrared thermography. Materials Letters 61, 747 – 750.

Mori, K., Spagnoli, A., Murakami, Y., Kondo, G., Torigoe, I., 2002. A new non-contacting non-destructive testing method for defect detection in concrete. NDT & E International 35, 399 – 406.

Sakagami, T., Kubo, S., 2002. Development of a new non-destructive testing technique for quantitative evaluations of delamination defects in concrete structures based on phase delay measurement using lock-in thermography. Infrared Physics & Technology 43, 311 – 316.

Spitznogle, F.R., Quazi, A.H., 1970. Representation and analysis of time-limited signals using a complex exponential algorithm. The Journal of the Acoustical Society of America 47, 1150–1155.

Sugimoto, K., Akamatsu, R., Sugimoto, T., Utagawa, N., Kuroda, C., Katakura, K., 2015. Defect-detection algorithm for noncontact acoustic inspection using spectrum entropy. Japanese Journal of Applied Physics 54, 07HC15.

Van Der Auweraer, H., Guillaume, P., Verboven, P., Vanlanduit, S., 2001. Application of a fast-stabilizing frequency domain parameter estimation method. Journal of dynamic systems, measurement, and control 123, 651–658.

Verboven, P., Cauberghe, B., Parloo, E., Vanlanduit, S., Guillaume, P., 2004. User-assisting tools for a fast frequency-domain modal parameter estimation method. Mechanical systems and signal processing 18, 759–780.

Zhu, J., Popovics, J.S., 2007. Imaging concrete structures using air-coupled impact-echo. Journal of engineering mechanics 133, 628–640.

Table 1: Summary of concrete mix proportions.

Water cement ratio (%)	Fine aggregate ratio (%)	Water (kg/m^3)	Cement (kg/m^3)	Fine aggregate (kg/m^3)	Coarse aggregate (kg/m^3)	Admixture (kg/m^3)
70	48	170	240	880	1000	0.60

Table 2: Estimated indicators for identified modes.

Mode	f_n (Hz)	ξ_n (%)
1	1220	1.01
2	1390	0.14
3	2090	0.52
4	2140	0.47
5	3150	0.39

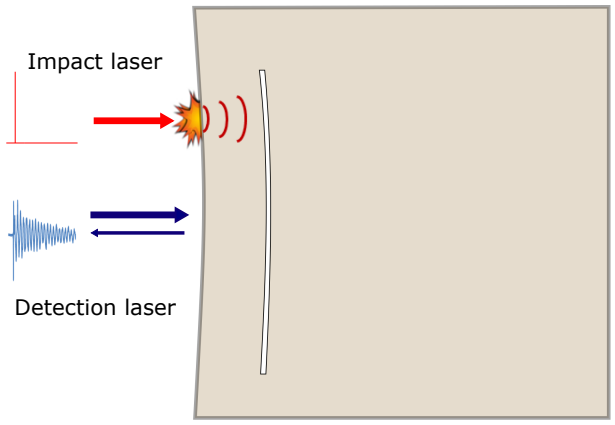

Figure 1: Schematic diagram of remote laser sensing method.

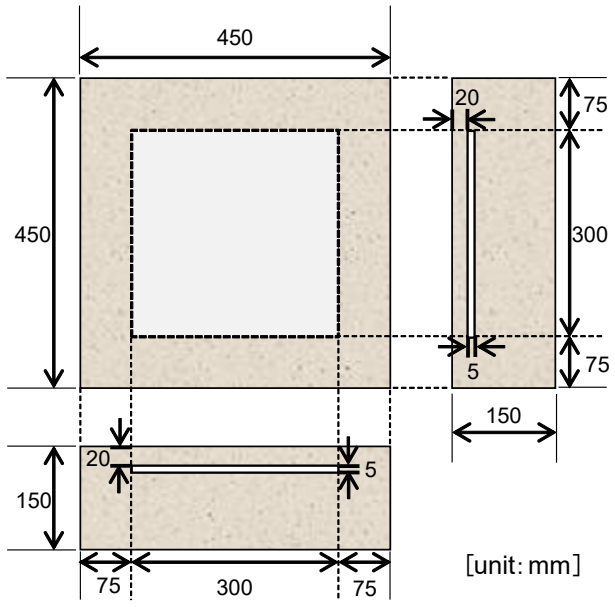

Figure 2: Dimensions of concrete specimen with an internal defect.

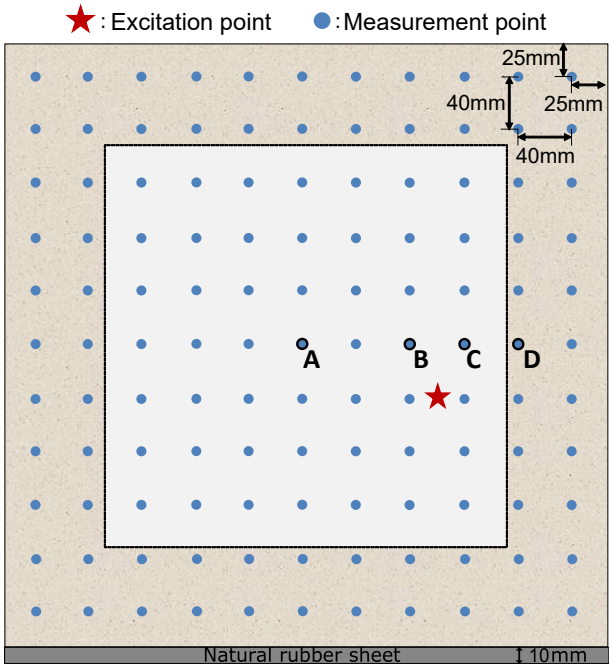

Figure 3: Impact point and measurement points on the concrete specimen.

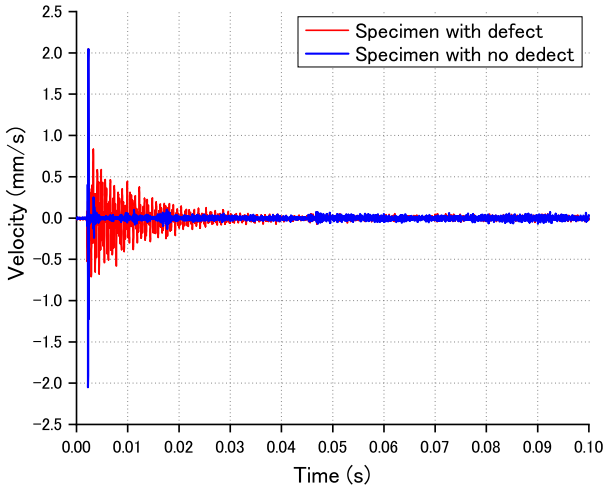

(a)

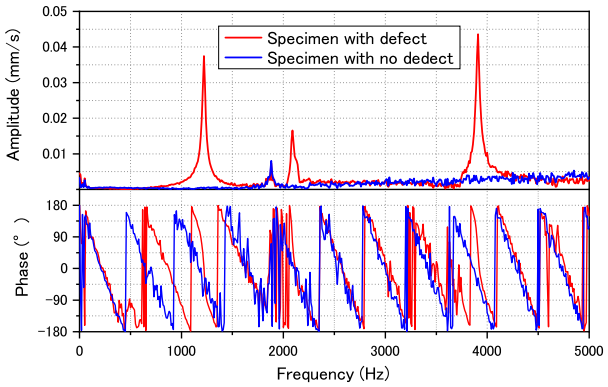

(b)

Figure 4: Comparison of laser-induced vibration of concrete specimen with an internal defect and the specimen with no defect at measurement point A. (a) Velocity waveform averaged over five measurements and (b) Fourier spectrum of the waveform.

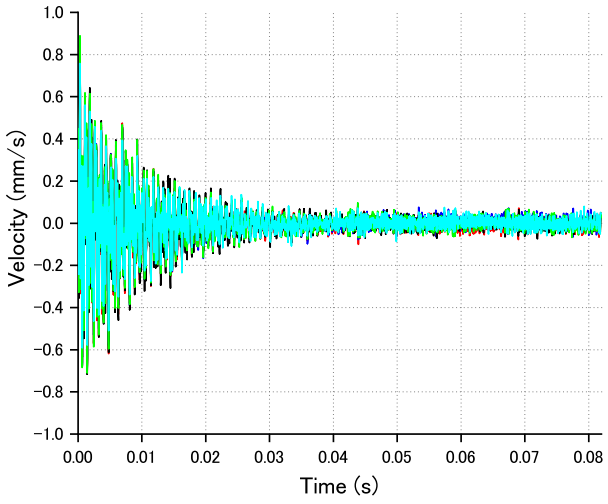

(a)

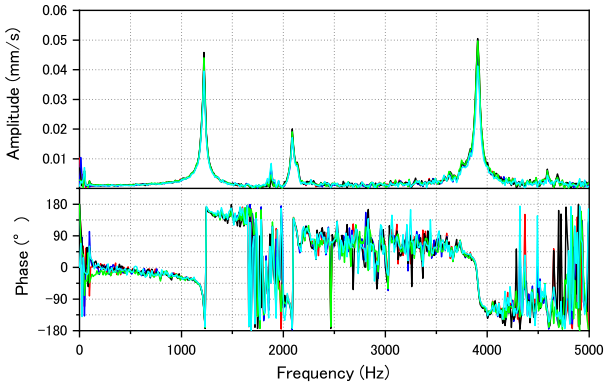

(b)

Figure 5: Laser-induced vibrations in concrete specimen with an internal defect at measurement point A. (a) Velocity waveforms for five measurements and (b) Fourier spectra of these waveforms. The data begins 0.0010 s after laser irradiation starts.

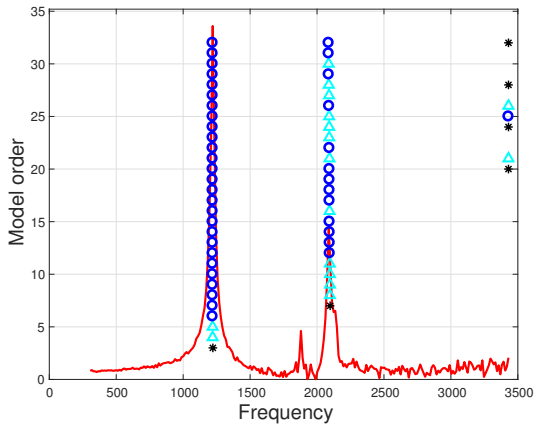

(a)

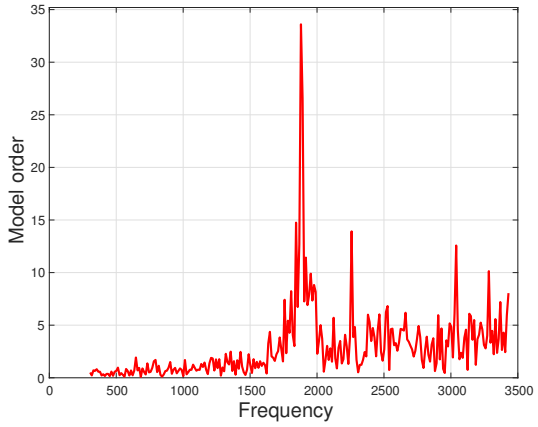

(b)

Figure 6: Stabilization diagrams at measurement point A for (a) the specimen with the internal defect and (b) the specimen with no internal defect.

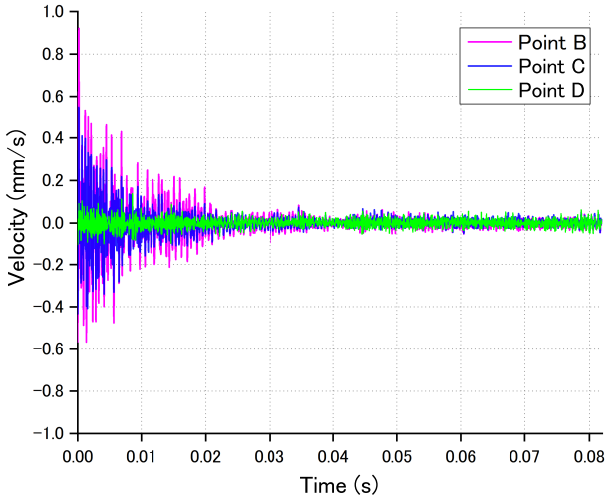

(a)

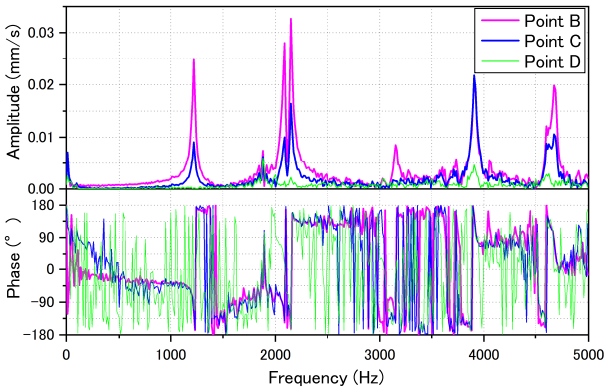

(b)

Figure 7: Results for laser-induced vibration in concrete specimen with an internal defect at measurement points B, C, and D. (a) Velocity waveforms averaged over five measurements and (b) Fourier spectra of these waveforms. The data begins 0.0010 s after laser irradiation starts.

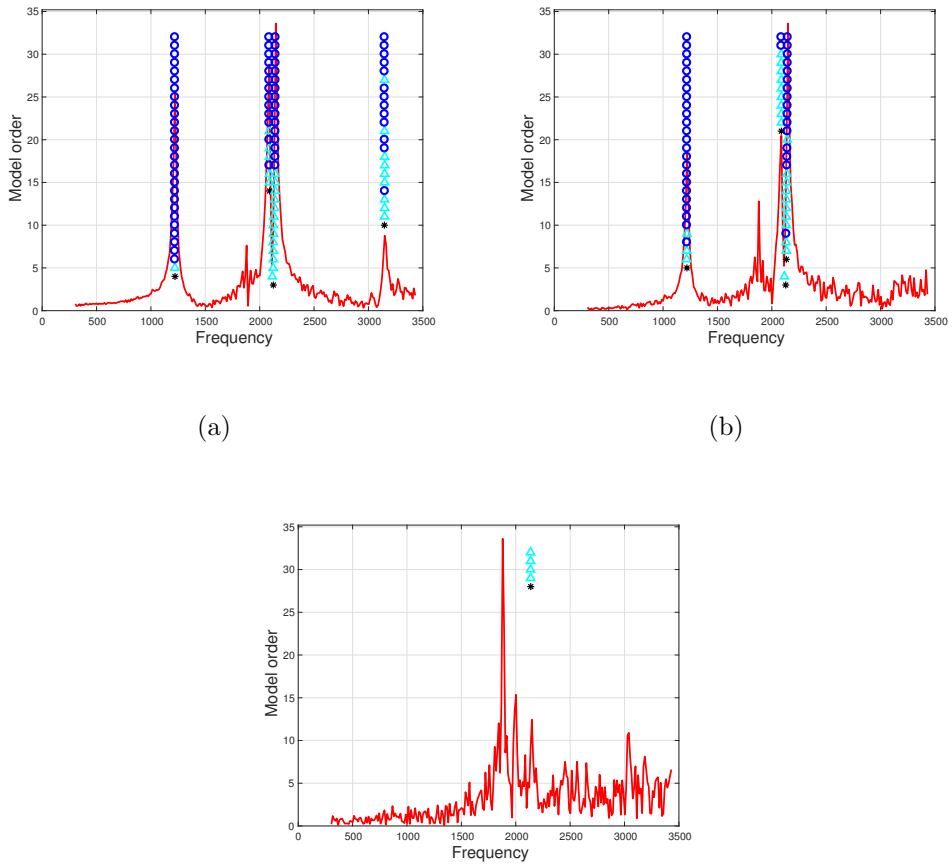

(a) (b)

(c)

Figure 8: Stabilization diagrams at measurement points (a) B, (b) C, and (c) D.

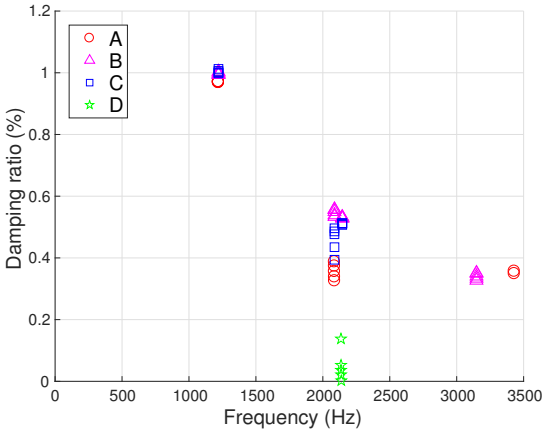

Figure 9: Distribution of estimated natural frequencies and damping ratio of the defect. The number of assumed modes N used for the calculations ranges from 28 to 32 for each point.

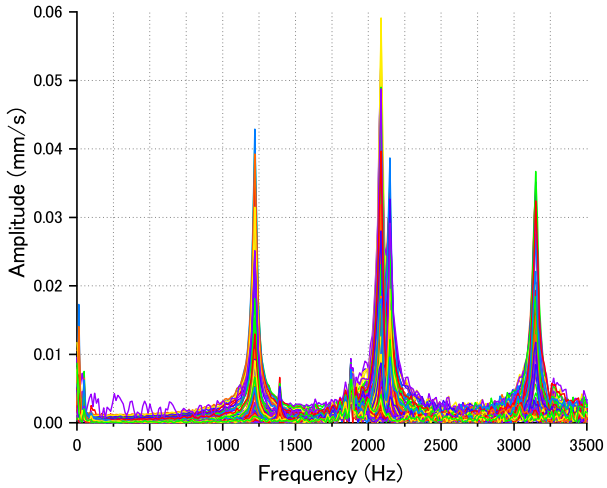

Figure 10: Fourier amplitude spectra for concrete specimen with an internal defect measured at all 121 points.

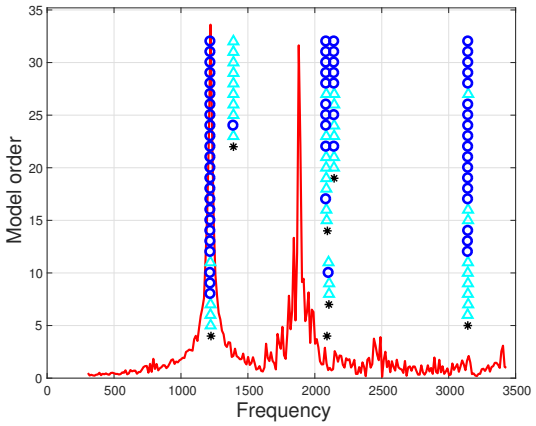

Figure 11: Stabilization diagrams derived from all 121 points.

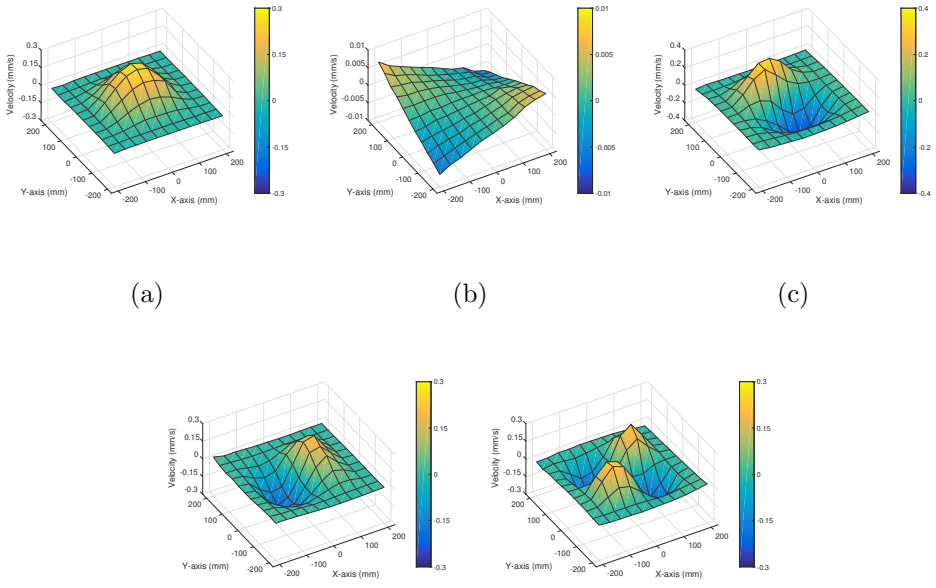

Figure 12: Estimated mode shapes: (a) mode 1, (b) mode 2, (c) mode 3, (d) mode 4, and (e) mode 5.

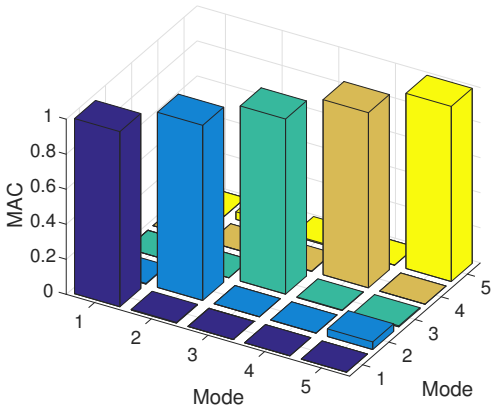

Figure 13: MAC values between each of the estimated modes.